Supporting Information for

Enhanced Tribological Performance of Supramolecular Gel with F-doped Carbon Dots via In-situ Directional Ultrasonication

Guangkai Jin,[a] Hang Li,[a] Yuhong Cui,[a] Tiantian Wang,[a] Shenghua Xue,[a] Junqin Shi,[a] Shujuan Liu,[a] Qian Ye,*[a] Feng Zhou*[ab] and Weimin Liu[ab]

[a]*State Key Laboratory of Solidification Processing, Center of Advanced Lubrication and Seal Materials, School of Materials Science and Engineering, Northwestern Polytechnical University, Xi'an, 710072, P. R. China.*

[b]*State Key Laboratory of Solid Lubrication, Lanzhou Institute of Chemical Physics, Chinese Academy of Sciences, Lanzhou, 730000, P. R. China.*

Keywords: F-doped carbon dots; supramolecular gel; directional ultrasonication; tribological properties; rheological performance

*Corresponding author: yeqian213@nwpu.edu.cn (Qian Ye), zhouf@licp.cas.cn (Feng Zhou)

CONTENTS

Experimental section

1. Materials

3-fluorobenzaldehyde (97% purity), acetaldehyde (35 wt% in water), sodium hydroxide (NaOH, GR grade) and the nonionic surfactant Span 80 were procured from Shanghai Aladdin. Dialysis membranes (Jiele Pu, dimensions: 44 mm × 28 mm, MWCO: 3500) were sourced from Hunan YiBo Biological Technology Co., Ltd. The base oil PAO, characterized by a viscosity of 117.6 mPa at 25℃ and a shear rate of 10 s^{-1}, was provided by the Lanzhou Institute of Chemical Physics, Chinese Academy of Sciences. The base oil PEG (Mn=380-420 g/mol) was acquired from Shanghai Chemical Reagent Company. Additionally, all water used in the experiments was deionized.

2. Characterization of F-CDs and Gel@F-CDs

Transmission Electron Microscope (Talos F200X) was used to obtain the microstructure and elemental composition information of CDs. X-ray diffractometer (D8, Advance) was applied to measure the crystalline properties of CDs. Fourier Infrared Spectroscopy (FTIR, TENSOR II) and X-ray Photoelectron Spectroscopy (XPS, PHI 5000 VersaProbe III) were taken to analyze the surface characteristic functional groups of CDs. Using a microconfocal Raman Spectrometer (WITec Alpha 300R) to obtain the characteristic D-peak and G-peak of CDs and measure the crystallization properties of CDs (excitation wavelength of 514 nm and beam diameter of 1.25 μm). The Zetasizer Nano Zeta Potential was employed to obtain the surface potential information of CDs (dispersed in H_2O, 25°C). The fluorescence spectra of CDs were measured by a Fluorescence Spectrometer (FLS 980, Edinburgh). The optical absorbance was determined by an UV-visible Spectrophotometer (LAMBDA 365). The Gel@F-CDs were crosscut by focused ion beam scanning electron microscope (FIB-SEM, Helios G4 CX), and then the 3D networks was captured by SEM.

3. Molecular Dynamics (MD) Simulation of the different oil samples

In order to analyze the significant differences in the physical properties of PAO solutions induced

by various additives, we constructed molecular dynamics (MD) simulation models, as depicted in **Fig. S11** and **Fig. S26-28**. The number of molecules in the models is detailed in **Table S2**. These models were subjected to 1 ns of equilibrium MD simulations under the NPT ensemble to achieve a liquid density closer to the actual state, with the temperature set at 298 K (25 ℃) and the pressure at 0.1 MPa.[1] Subsequently, the simulations were converted to the NVT ensemble while maintaining the same temperature for an additional 1 ns to statistically analyze the diffusion process of PAO. The OPLS-AA force field was employed for all lubricant molecular simulations, owing to its extensive application in various organic systems.[2] The cutoff distance for van der Waals forces was set at 10 Å, and the long-range electrostatic interactions with an accuracy of 10^{-4} were calculated using the particle-particle particle-mesh (PPPM) method.[3] Throughout all simulations, the temperature at 298 K was controlled by the Nose-Hoover thermostat, while the velocities were integrated using the Verlet algorithm to solve the equations of motion with a time step of 1 fs. Periodic boundary conditions were applied in all three directions of the model. The simulations were conducted using the open-source simulation code LAMMPS,[4] and the configurations were visualized with the OVITO software.[5]

4. Rheological properties of Gel@F-CDs

The gel's antioxidant properties were assessed using Thermogravimetric analysis (TGA, STA 449F3), while its phase transition temperature was determined through Differential Scanning Calorimetry (DSC). TGA under N_2 atmosphere (35~800 ℃, 10 ℃/min) was used to study the stability of pure PAO and Gel@F-CDs. The rheological properties of Gel@F-CDs were evaluated using a HAAKE MARS III rheometer at a constant temperature of 25 ℃. The viscosity measurements were obtained at a shear rate of 10 s^{-1} with the weight of about 200 mg. At a frequency of 1 Hz, we determined the functions of storage modulus (G′) and loss modulus (G″) as they vary with increasing shear stress from 0.1 to 1000 Pa. Under a constant shear stress of 1 Pa, the

variation of G′ and G″ with frequency was recorded. Additionally, the rheological behavior of Gel@F-CDs with varying mass fractions of F-CDs was examined in response to changes in shear rate. Ultimately, we conducted creep recovery and fast-slow shear cycling tests on the gel. These tests involved shear rates of 300 s^{-1} and 1 s^{-1}, with each rate sustained for 100 seconds in a cycle repeated four times.

5. Tribological performance of Gel@F-CDs

The tribological performance test was performed on the SRV-V test machine, using the contact mode of the ball-on-disk. The upper ball (ø 10 mm, 60 ± 2 HRC, mean roughness 20 nm) and the lower disk (ø 24 mm ×7.9 mm, 62 ± 2 HRC) were both made of AISI 52100 steel. The steel ball and steel disk were respectively held in a special clamp and absolutely stationary on the table to ensure that the disk did not slip relative to the fixture during high-frequency vibration. The test conditions were as follows: constant load test (150 N, 50 °C, 25 Hz, 1 mm); varying frequency test (150 N, 50 °C, 1 mm, frequency from 5 Hz to 50 Hz, increase by 5 Hz every 5 min); varying temperature test (150 N, 25 Hz, 1 mm, temperature from 40 °C to 120 °C, increase by 10 °C every 5 min); varying load test (50 °C, 25 Hz, 1 mm, load from 50 N to 1000 N, increase by 50 N every 5 min). The wear volume and wear depth of the worn surface on disk were observed by three-dimensional (3D) surface profiler (Bruker, NPFLEX). SEM (Field Emission Scanning Electron Microscopy, TESCAN) was used to obtain the microstructure of the worn surface and analyze the mechanism.

For the constant applied load, the corresponding mean Hertz pressure P can be calculated by the follow equation in the Hertz contact zone:

$$P = \frac{1}{\pi}\sqrt[3]{\frac{16W\left(E^{※}\right)^2}{9\left(R^{※}\right)^2}}$$

W is the applied load.

$E^{※}$ is the elastic modulus of the system. And $\frac{1}{E^{※}} = \frac{1-\gamma_1}{E_1} + \frac{1-\gamma_2}{E_2}$

E_1 and E_2 are the elastic modulus of the ball and disk, respectively. And γ_1 and γ_2 are the Poisson's ratio of the ball and disk, respectively.

$R^{※}$ is the elastic modulus of the system. And $\frac{1}{R^{※}} = \frac{1}{R_1} + \frac{1}{R_2}$

R_1 and R_2 are the radius of curvature of the ball and disk, respectively.

In our experiment, under constant conditions, the W is 150 N, $E_1 = E_2$=210 GPa, $R_1 = 5\ mm$ and $R_2 = \infty$.

So,

$$P = \frac{1}{\pi}\sqrt[3]{\frac{16W(E^{※})^2}{9(R^{※})^2}} = \frac{1}{\pi}\sqrt[3]{\frac{16 \times 150 \times \left(\frac{210 \times 10^9}{2 \times (1-0.3^2)}\right)^2}{9 \times (5 \times 10^{-3})^2}} = 1.661 \times 10^9\ (Pa)$$

So, the mean Hertzian pressure for the loads applied is about 1.661 GPa.

The detailed calculations pertaining to Hertzian stresses have been appended to the supplementary information, facilitating future researchers in their investigation of the load-bearing capacity of nanoscale additives.

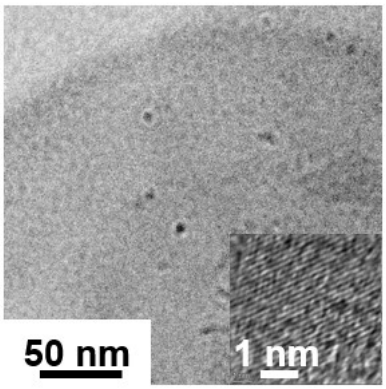

Fig. S1. The HR-TEM image of F-CDs.

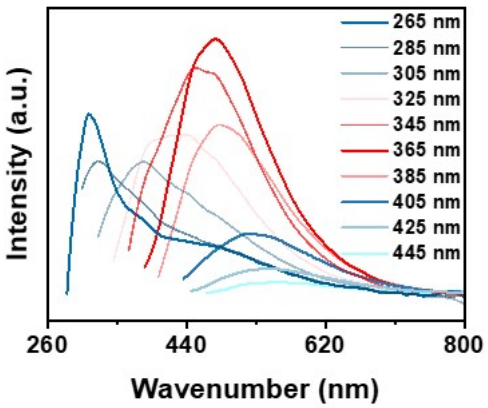

Fig. S2. The excitation-dependent PL spectra of the Gel@F-CDs.

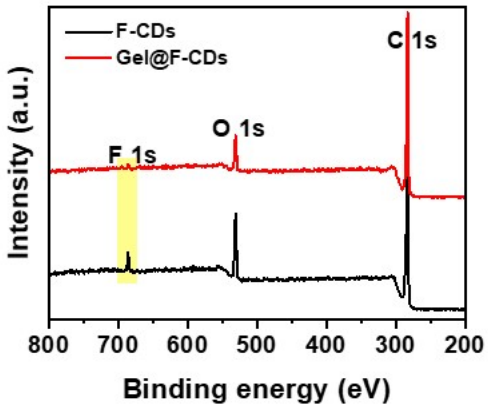

Fig. S3. The XPS full spectra of F-CDs and Gel@F-CDs.

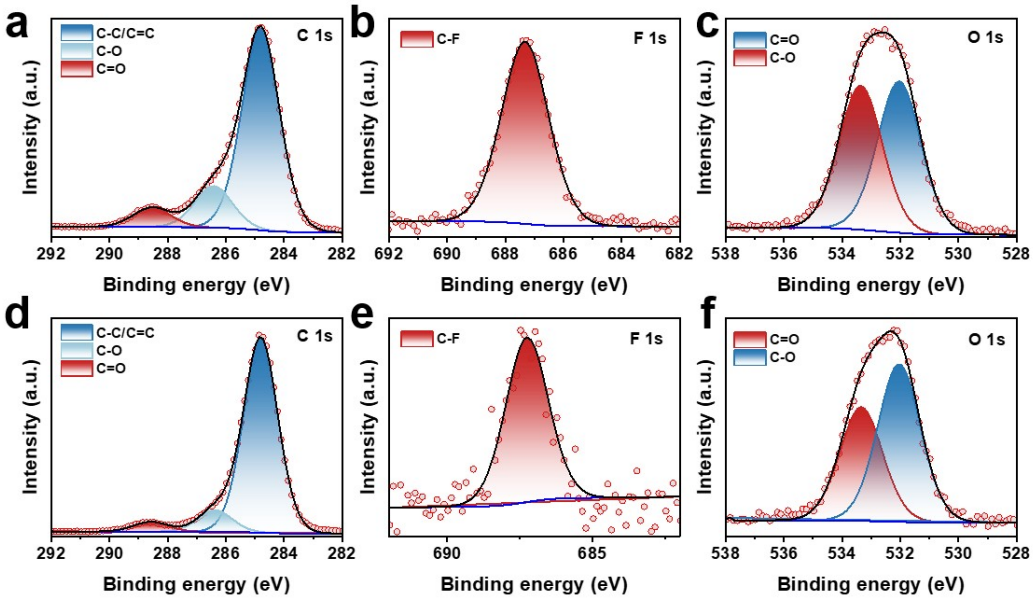

Fig. S4. The XPS fine spectra of the C 1s, F 1s and O 1s of the (a-c) F-CDs and (d-f) Gel@F-CDs.

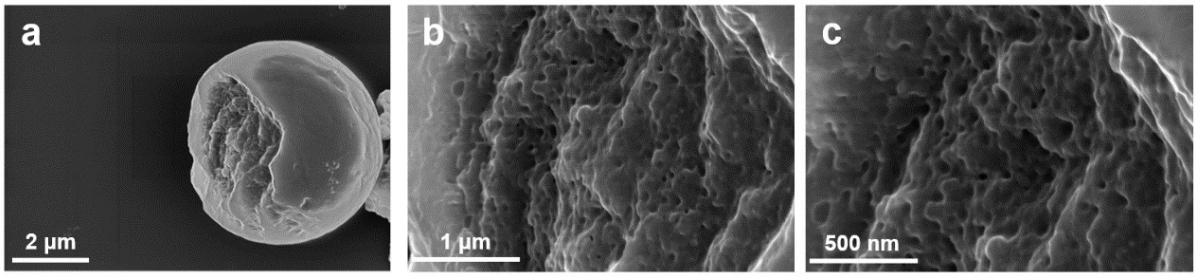

Fig. S5. The SEM images of the 3D networks of the Gel@F-CDs.

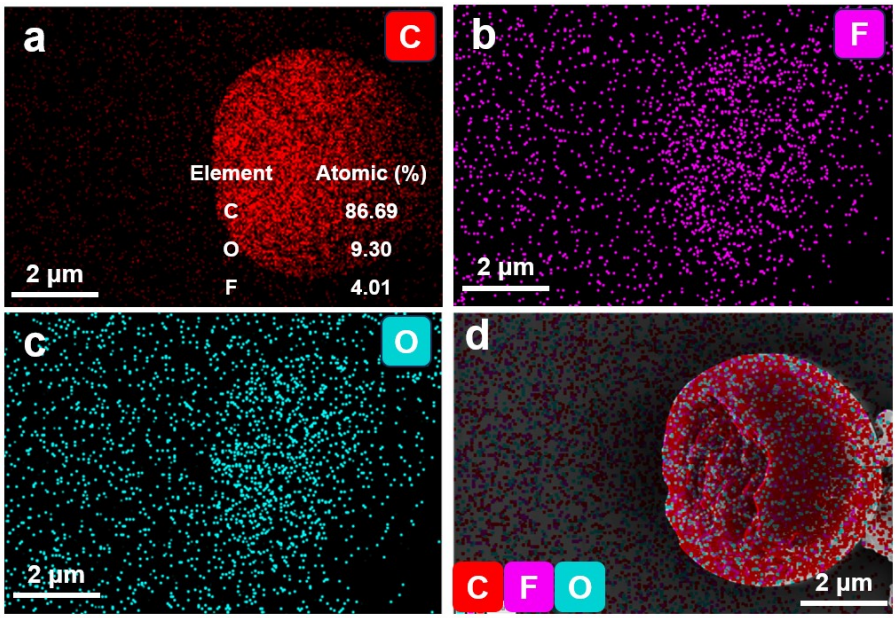

Fig. S6. The element mappings of (a) C, (b) F, (c) O and (d) the combination of C, F and O of the Gel@F-CDs.

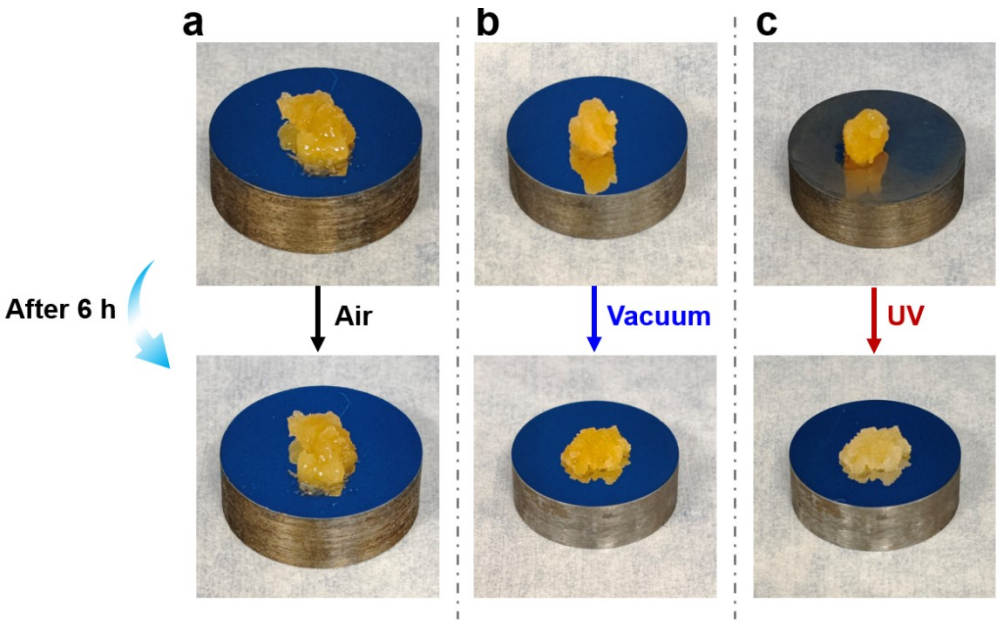

Fig. S7. The anti-creep behavior of the Gel@F-CDs under the different environments in the (a) air, (b) vacuum and (c) UV light.

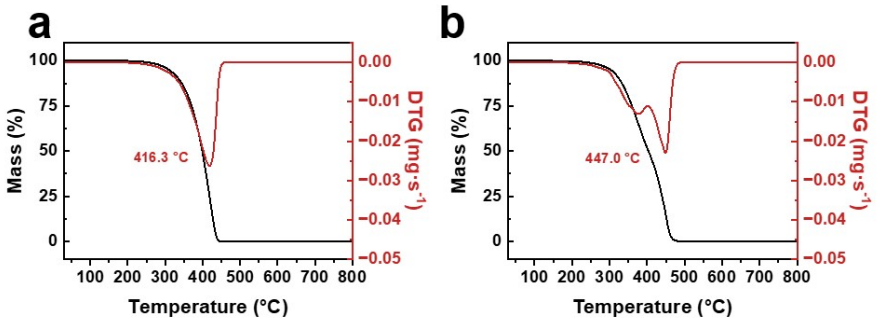

Fig. S8. The TG curves and the DTG curves of the base oil PAO (a) and Gel@F-CDs (b).

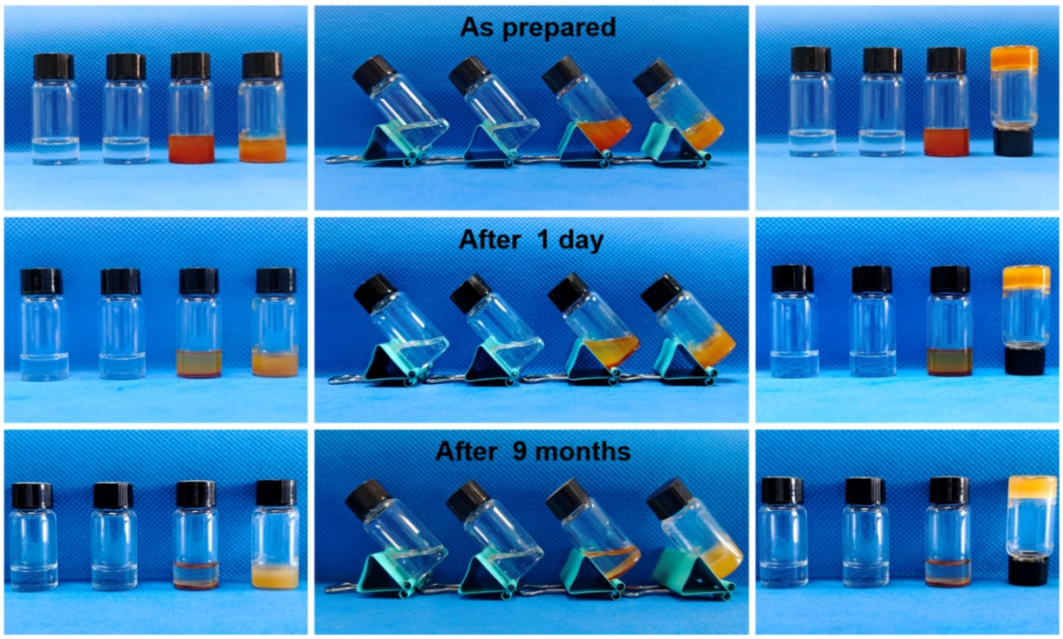

Fig. S9. The optical images of the different samples (from left to right: PAO, PAO+3 wt% Span, PAO+3 wt% F-CDs and Gel@F-CDs) of the dispersion stability testing (vertical, inclined and inverted placement of images).

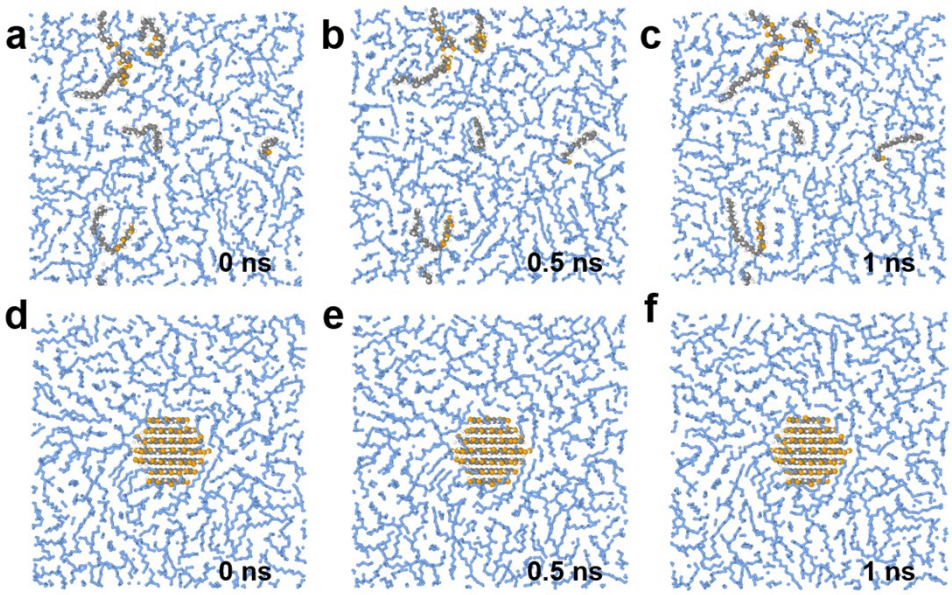

Fig. S10. The results of molecular dynamics simulation: Side view of the PAO+Span (a-c) and PAO+F-CDs (d-f) at different moments (0 ns, 0.5 ns and 1 ns).

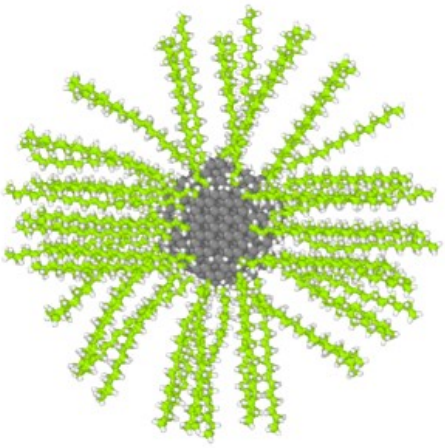

Fig. S11. The structure of gelling agent of Gel@F-CDs in simulation.

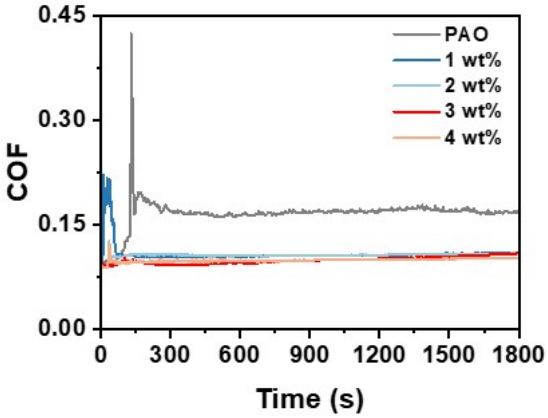

Fig. S12. The COF curves of the Gel samples containing different amount of F-CDs.

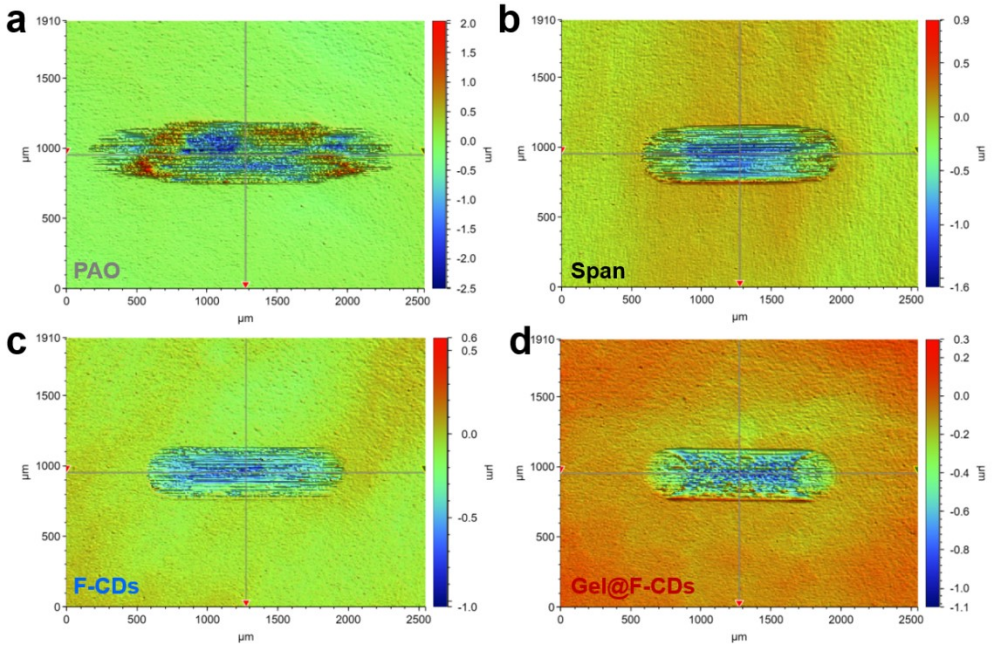

Fig. S13. The images of the lower disk lubricated by the samples: (a) base oil PAO, (b) PAO+Span, (c) PAO+F-CDs and (d) Gel@F-CDs.

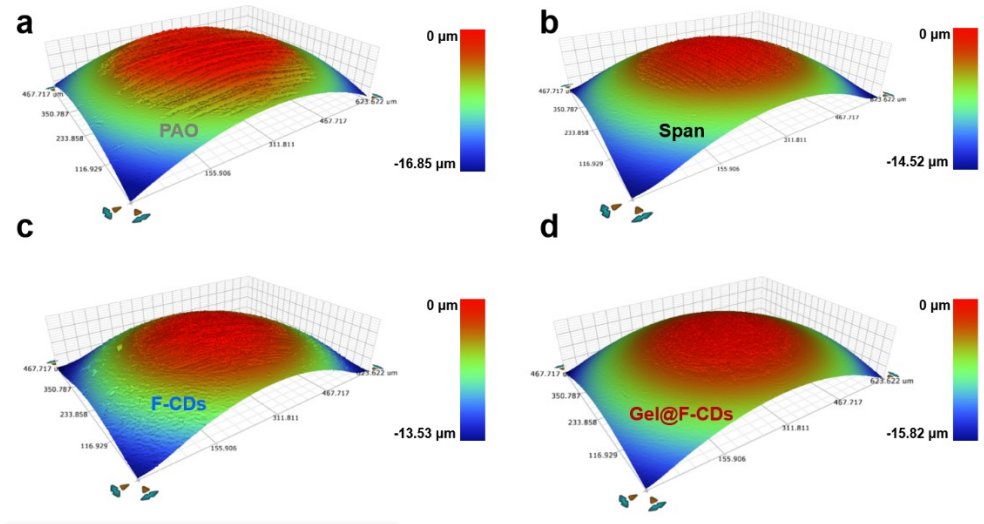

Fig. S14. The 3D images of the upper ball lubricated by the samples: (a) base oil PAO, (b) PAO+Span, (c) PAO+F-CDs and (d) Gel@F-CDs.

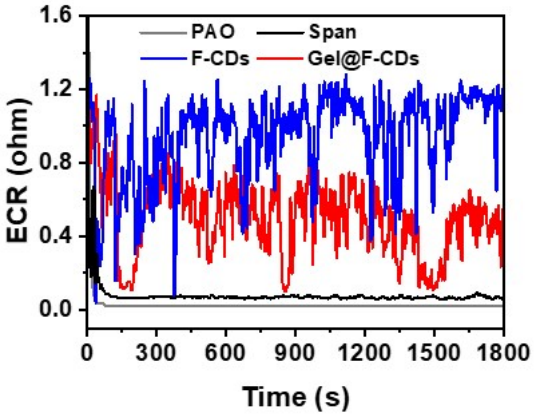

Fig. S15. Average electrical contact resistance measurement of the different samples.

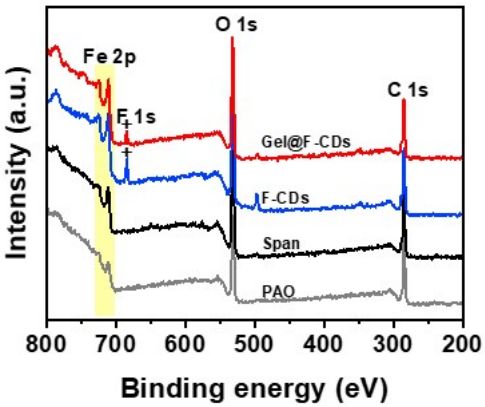

Fig. S16. The XPS full spectra of the worn surface lubricated by different samples.

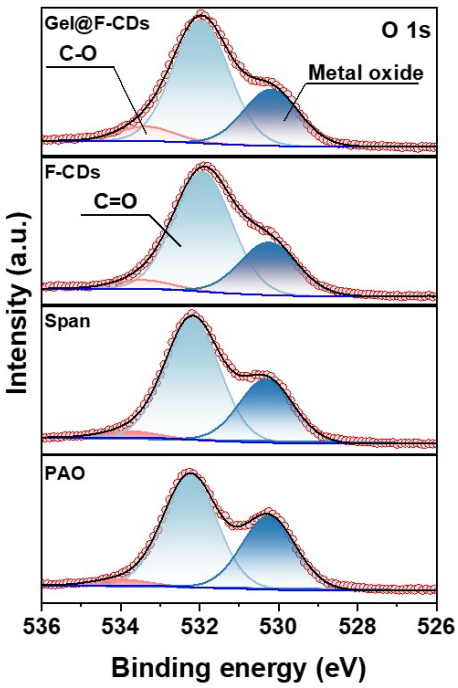

Fig. S17. The XPS fine spectra of O 1s on the worn scar of the lower disk lubricated by different samples.

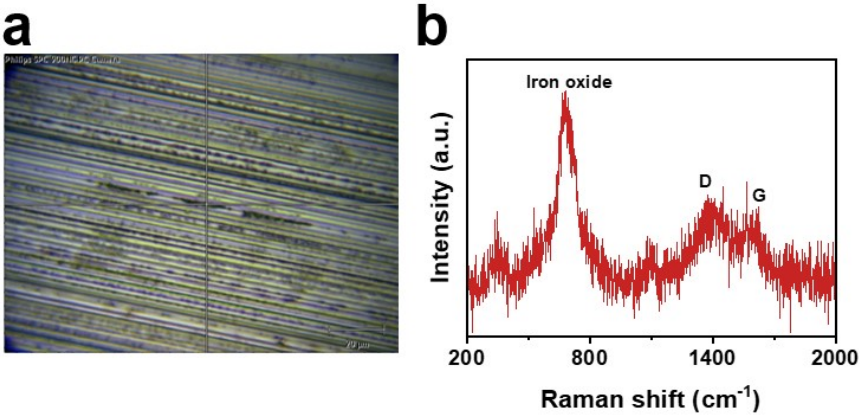

Fig. S18. (a) The Raman optical image (captured by CCD) and (b) the Raman spectrum of the worn surface lubricated by the Gel@F-CDs.

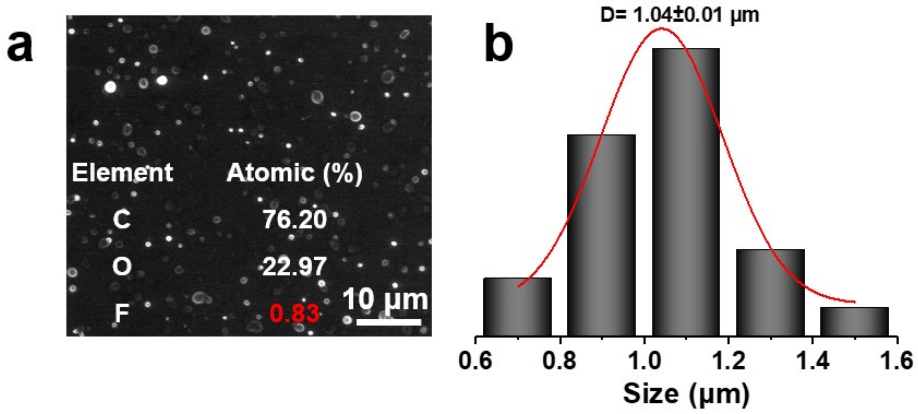

Fig. S19. (a) The SEM images of the Gel@F-CDs and (b) their size distribution after the tribological experiments.

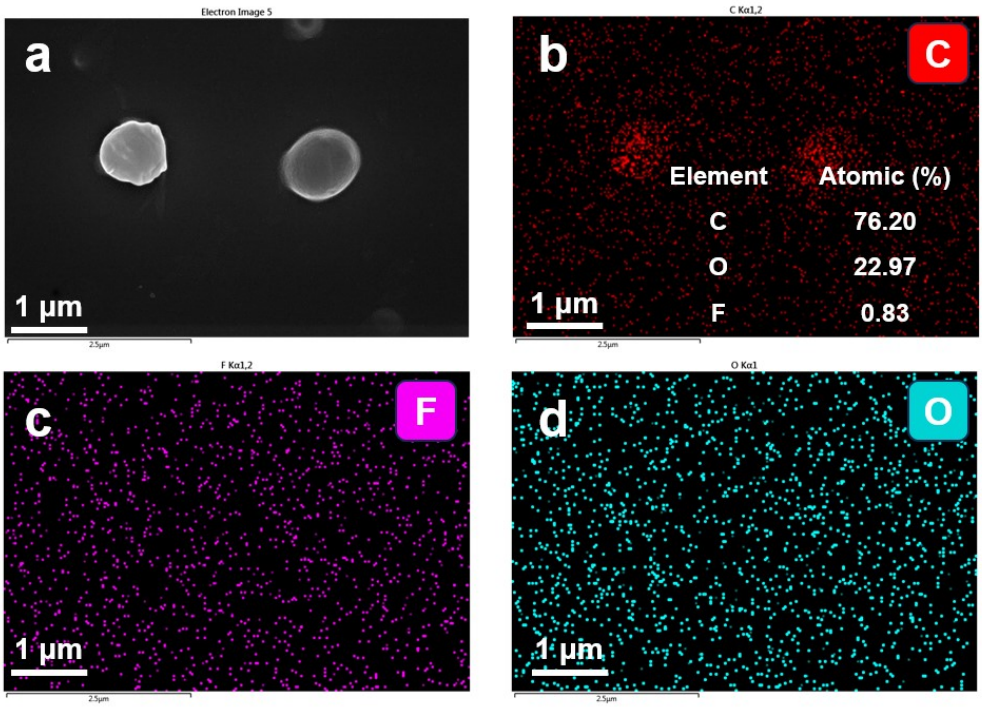

Fig. S20. (a) The SEM images and (b-d) the element mappings of the Gel@F-CDs after the tribological experiments.

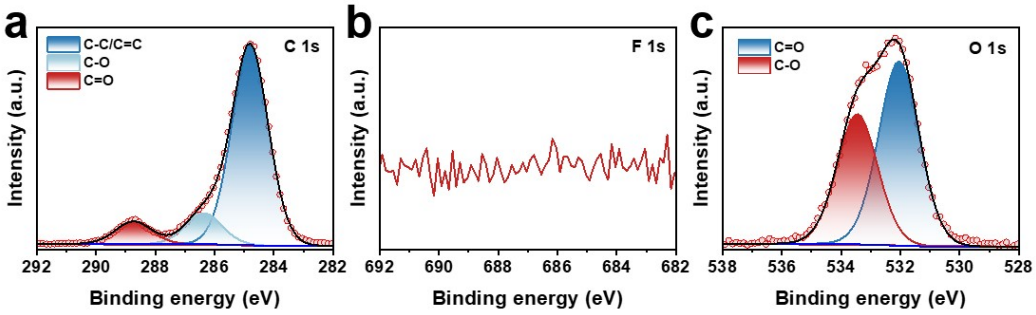

Fig. S21. The XPS fine spectra of the (a) C 1s, (c) F 1s and (d) O 1s of the Gel@F-CDs after tribological experiment.

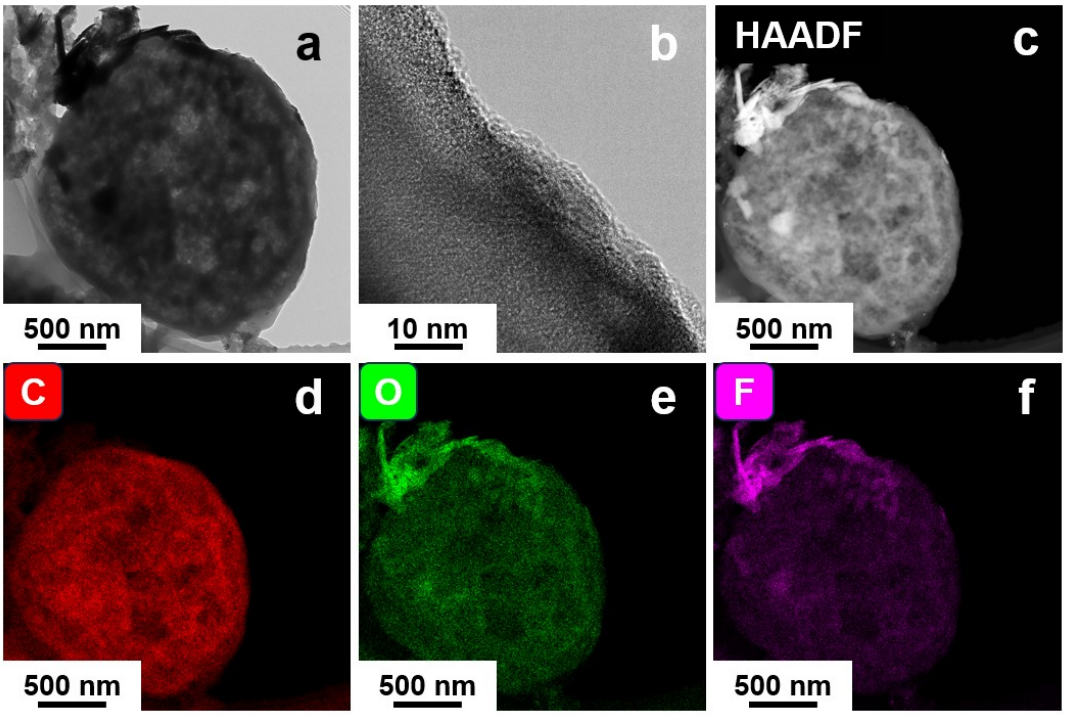

Fig. S22. (a-b) the TEM images and (c-f) the element mappings of the Gel@F-CDs after the tribological experiments.

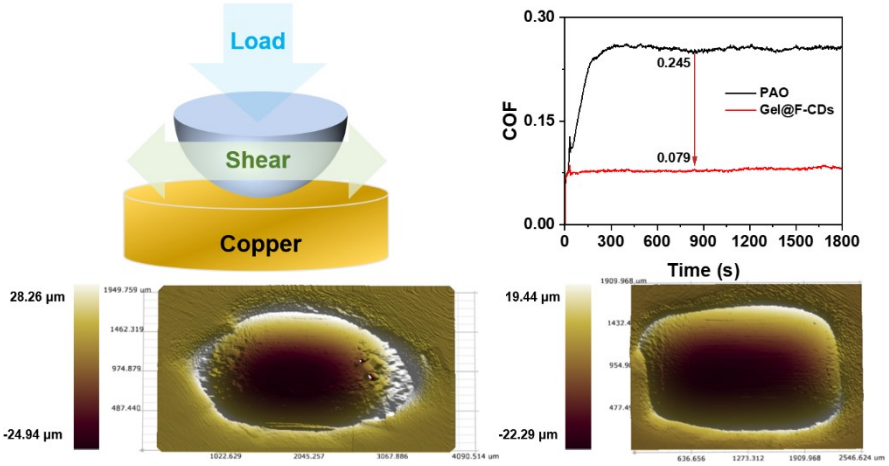

Fig. S23. Tribological properties of the as-prepared samples at a load of 150 N, 50 °C, 25 Hz (friction pair: steel ball vs copper disk).

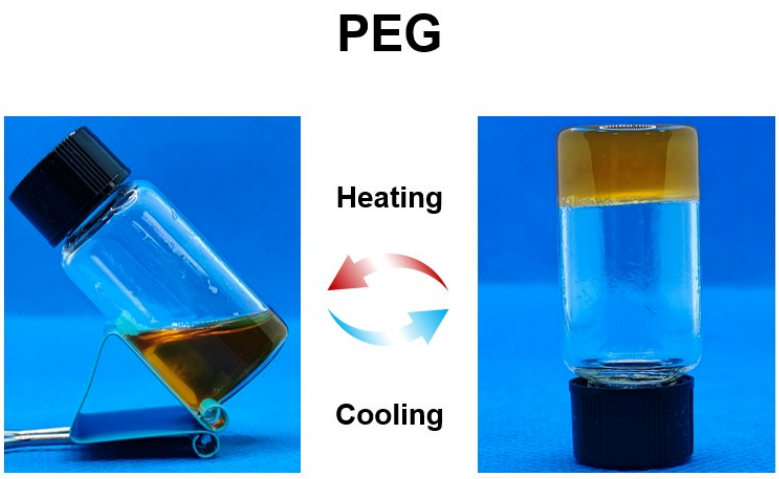

Fig. S24. The Gel@F-CDs in PEG with heat-cooling cycle.

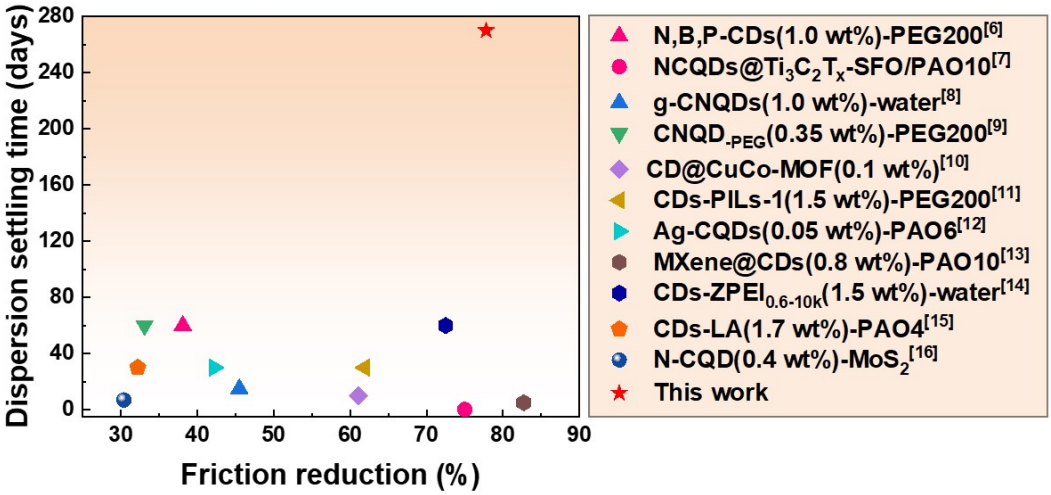

Fig. S25. Tribological performance of CDs as lubricant additives in liquid lubrication.

6-16

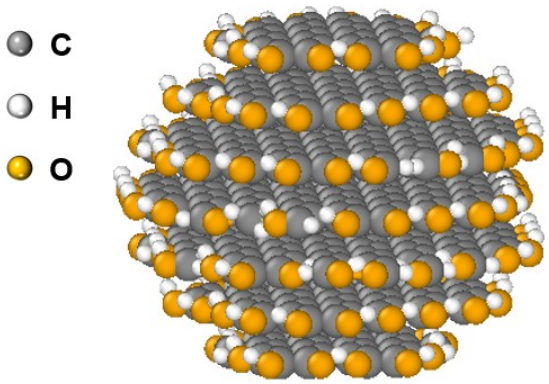

Fig. S26. The structure of CDs in simulation.

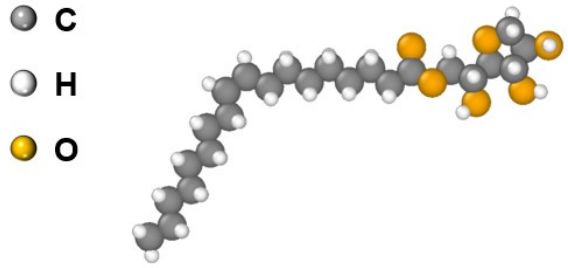

Fig. S27. The structure of Span in simulation.

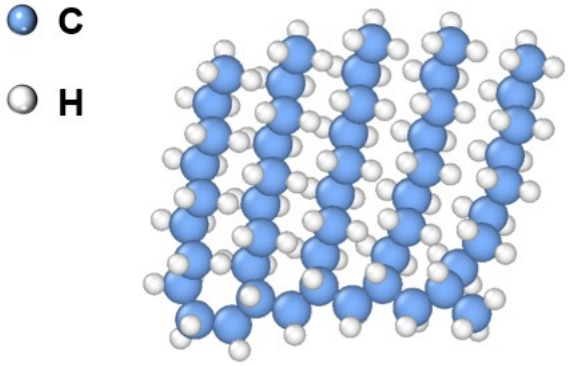

Fig. S28. The structure of PAO in simulation.

Table S1. The element content of the worn surface lubricated by different samples (atomic percentage).

	C	O	F	Fe
PAO	67.46	31.20	/	1.34
PAO+Span	61.55	36.28	/	2.17
PAO+F-CDs	56.97	36.74	3.14	3.16
Gel@F-CDs	55.06	38.42	2.01	4.52

Table S2. Molecular model used in molecular dynamics simulation.

	Span	F-CDs	Gel@F-CDs	PAO
Model 1	20	/	/	300
Model 2	/	1	/	300
Model 3	/	/	1	300

Reference

1. G. J. Martyna, M. L. Klein and M. Tuckerman, *J. Chem. Phys*, 1992, **97**, 2635-2643.
2. W. L. Jorgensen, David S. Maxwell and J. Tirado-Rives, *J. Am. Chem. Soc*, 1996, **118**, 11225-11236.
3. S. Stephan, S. Schmitt, H. Hasse and H. M. Urbassek, *Friction*, 2023, **11**, 2342-2366.
4. S. Plimpton, *J. Comput. Phys.*, 1995, **117**, 1-19.
5. A. Stukowski, *Modell. Simul. Mater. Sci. Eng.*, 2010, **18**, 015012.
6. W. Zhu, Y. Tan, W. Tang, Y. Li and Y. Tang, *Diam. Relat. Mater.*, 2023, **139**, 110315.
7. D. Wang, X. Jia, Y. Zhang, Z. Shan, J. Yang, Y. Su and H. Song, *Tribo. Int.*, 2023, **190**, 109023.
8. W. Tang, Y. Wang, X. Zhu, Z. Zhang, W. Zhu, H. Liu, W. Gao and Y. Li, *Wear*, 2023, **528-529**, 204950.
9. W. Tang, H. Liu, W. Zhu and X. Wei, *Carbon*, 2023, **207**, 305-316.
10. J. Wang, D. Tian, T. Yan, W. Liang, L. Zhang, X. Li and S. Gao, *Appl. Surf. Sci.*, 2023, **641**, 158477.
11. Z. Mou, B. Wang, H. Lu, S. Dai and Z. Huang, *Carbon*, 2019, **154**, 301-312.
12. J. Wang, X. Li, Y. Deng, S. Chen, W. Liang, L. Zhang, X. Wei, S. Gao and Y. Wan, *Appl. Surf. Sci.*, 2022, **599**, 154029.
13. Y. Cui, S. Xue, S. Wang, X. Chen, S. Liu, Q. Ye, F. Zhou and W. Liu, *Carbon*, 2023, **205**, 373-382.
14. Z. Mou, R. Yan, J. Peng, Y. Li, Z. Huang, Z. Wang, B. Zhao and D. Xiao, *Chem. Eng. J.*, 2023, **465**, 142986.

15. Z. Zhang, J. Zhao, X. Li and B. Wang, *Diam. Relat. Mater.*, 2024, **141**, 110715.

16. J. He, J. Sun, J. Choi, C. Wang and D. Su, *Friction*, 2022, **11**, 441-459.